An experimental study of the flow through and over two dimensional rectangular roughness elements: Deductions for urban boundary layer parameterizations and exchange processes

M. K.-A. Neophytou[1,*], C. N. Markides[2] and P. A. Fokaides[1]

[1] *Environmental Fluid Mechanics Laboratory, Department of Civil and Environmental Engineering, University of Cyprus, P.O. Box 20537, 75 Kallipoleos Ave., 1678 Nicosia, Cyprus*

[2] *Department of Chemical Engineering, Imperial College London, South Kensington, London SW7 2AZ, UK*

Abstract

This paper investigates the flow through and over two-dimensional rectangular roughness elements arranged in a building-street canyon geometry through a series of experiments. Geometries of different packing densities of the roughness elements (λ_p) were examined and the packing density values ranged from λ_p = 0.30 to 0.67. The purpose of the work is: (i) to investigate the flow physics observed both at the boundary layer scale as well as at the scale within the roughness elements for a range of packing densities (ii) to deduce parameterizations of the adjusted rough boundary layer and their variation with a change in the packing density , and (iii) given a particular interest in and application to the urban atmosphere, a final aim at the roughness-element scale is to deduce the variation of the breathability with the packing density variation.. Particle Image Velocimetery measurements of the velocity flow field as well as the turbulent kinetic energy and the Reynolds Stress (within and up to well-above the street canyons) were conducted. The results reveal qualitative flow features as well as features of the adjusted boundary layer structure - in particular the roughness and inertial sublayers, which can be associated with the surface roughness length, zero-plane displacement thickness and the friction velocity. The lowest friction velocities are exhibited in the geometries with the highest- and lowest-packing densities while the maximum friction velocities are observed in the medium-packed geometries. . The exchange processes and breathability at the level of the roughness elements top were characterized and quantified by a mean exchange velocity. The results show that unlike friction velocity, the normalized exchange velocity (over the mean bulk velocity) for the most dense and sparse geometries differ by more than 80%, with the denser-packed geometries exhibiting lower exchange velocities; this is shown to be related with the thickness of the developed roughness sublayer.

* Corresponding author. Email: neophytou@ucy.ac.cy; Tel: +357 2289 2266; Fax: +357 2289 5323

I. INTRODUCTION

The flow over rough surfaces is addressed in a diverse range of problems - from the fundamental understanding of boundary layer aerodynamics[1,2] to practical applications in, amongst other, drag reduction[3,4], atmospheric[5] and geophysical flows[6]. The motivation in such studies is primarily directed towards a scale of observation that is much larger than the scale of the roughness elements, and the results are primarily concerned with the macroscopic effect of the roughness elements on the flow well-above – be it friction or drag on the rough surface. The flow and transport processes that occur in the urban atmosphere, however, are addressed at various spatial (and temporal) scales, ranging from the *local* to the *global* scales[7,8]. At larger scales of observation (e.g., the city scale and above) the wind flow is considered as an atmospheric boundary layer flow over a rough surface, with the flow becoming more complex when topographical and terrain effects are also included[9,10]. At smaller scales of observation (e.g., at the street-canyon or neighbourhood scale) the buildings cannot be treated as surface roughness elements, but instead, as a group of obstacles – with the flow, as a result, having a completely different form and structure than that of a boundary layer.

A. The boundary layer scale

The wind profile over an urban area or a city can be treated by boundary layer formulae deriving from the general boundary layer theory, as long as the mean building height is small compared to the surface boundary layer depth and the surface has some statistical homogeneity. The horizontal wind-speed profile conforms to the Monin-Obukhov similarity theory, with the friction velocity (u^*) as the key scaling velocity, and two additional scaling lengths, the surface roughness length (z_0) and the zero-plane displacement thickness (d_0). For neutral or adiabatic conditions the wind-speed profile can be described by:

$$U = \frac{u^*}{\kappa} \ln\left(\frac{z - d_0}{z_0}\right) \tag{1}$$

where κ is the von Karman's constant taken to be 0.4. Estimates of the surface roughness length z_0 and the displacement length d_0 for an urban area can be made using information about urban morphology – the building sizes and spacing. The planar area index, λ_p, and frontal area index, λ_f, used by Grimmond and Oke[11] and others are used to classify the urban areas morphology and its density; it is noted that for square street canyons or cubical arrays, $\lambda_p = \lambda_f$. Despite the fact that the flow velocity follows a logarithmic profile at higher scales, it is unclear how it behaves in the layer closer to the surface that is influenced by the buildings[1] and more importantly how the adjusted profile above yields as a result of the building roughness elements below.

An atmospheric boundary layer over an urban area is composed, like most boundary layers over a rough surface, of an inertial sublayer (ISL) and a roughness sublayer (RSL). In the ISL, the fluxes are almost constant with height, and the profiles of mean quantities are logarithmic in neutral conditions; energy, momentum and mass fluxes are parameterized using the Monin-Obukhov similarity theory while the boundary layer thickness (or height) is much larger than the scale of the buildings. Turbulent diffusion is the dominating mechanism for scalar and momentum transfer and the behaviour of turbulence in this layer is governed by the background atmospheric conditions as well as the underlying urban surface. In this viewpoint, it is the flow in this inertial layer that is

characterized and thereby parameterized by the corresponding macroscopic urban aerodynamical parameters – the surface roughness length, z_0, the zero-displacement height, d_0, and the friction velocity, u^*[12,13].

In the RSL the flow is spatially varying, as it is affected by the individual roughness elements. A unified framework of description of flow variables has not yet been established – neither in the general boundary layer theory over rough surfaces nor in the context of urban atmosphere. The buildings forming the urban area cannot be treated simply as a surface roughness, and the flow cannot be simplified to that of a boundary layer. In fact the extent of the RSL covers two regimes: a regime of strong shear (the shear sublayer) extending from above the roughness-element top or rooftop level (i.e. at $z = z_H$) to some height further above into the atmospheric flow, at $z = z_r$; there is also a second regime, the regime of canyon circulation (canyon sublayer) which extends from the ground ($z = 0$) up to the rooftop level ($z = z_H$). The shear sublayer is induced by the drag of the roughness elements, in which their direct dynamic effects on turbulence are apparent. Any scalar transfer between the canyon sublayer and the ISL is influenced by this shear sublayer. Observations indicate that the RSL height, z_r, may vary; according to Cheng and Castro[14], when the wind profile is spatially averaged the logarithmic layer extends right down to the rooftop level, indicating that $z_r \approx z_H$.

To describe rough-wall turbulent boundary layer flows, friction velocity is customarily used as a non-dimensionalizing velocity for the mean velocity profile and the turbulence levels. In the context of atmospheric boundary layer flows and meteorological applications in particular, experimental studies in the laboratory have used instead a reference velocity at a pre-specified height (with respect to the roughness-element height). The attractiveness of the use of a friction velocity over that of a mean velocity at a reference height is that it does not require the specification and retention of a reference height; however a disadvantage is that it is not easy to measure and more importantly there is no consensus as to how to determine it, particularly for roughness elements – and even to a greater extent when roughness elements are in the form of urban-like geometries.

Although atmospheric flows are subject to many processes not found in the laboratory, there is no discussion on what an appropriate friction velocity would be in the context of urban geometries. Moreover, meteorological data, due to the height limitation of measurement towers, are often obtained in the RSL, and thereby likely to be inappropriate for overall parameterizations. Therefore, the understanding of atmospheric boundary layers has leaned heavily on experimental measurements in the laboratory aiming to understand better the atmospheric boundary layer structure [15], the turbulence structure[16], statistics[17,18], similarity[19] as well as the critical roughness height[20]. A wind tunnel study [21,22,23] addressing an urban boundary layer over a modelled real urban area found that the shear stress profiles show pronounced maxima in the flow region immediately above rooftop level and proposed a shear-stress parameterization based on the experimental data. A number of field studies have also addressed the urban boundary layer[24,25,26, 27], identifying some important aspects of flow and turbulence characteristics in the urban RSL; however , there are still open questions concerning appropriate scaling concepts and a lack of high resolution datasets[23]. Currently, there are no available laboratory measurements addressing the flow within roughness elements and connecting it systematically to the RSL and ISL of the adjusted boundary layer above. Such experiments would also serve recent relevant computational studies[21] that use similar geometries.

B. The roughness-element scale

At the roughness-element scale, or the building scale, the flow is often regarded as a flow channelling through a

network of streets[28], while air flow exchange processes occur between the in-canyon and above-canyon flows[29,30]. These exchange processes are important, because they relate to the capacity of a city to 'ventilate' itself, or more appropriately termed for this type of problems, to 'breathe'. The *breathability* of a city essentially relates to its capacity to remove pollutants, heat, moisture and any other scalars produced within the city[31]. This capacity also results in a momentum flux exchange which is balanced by the drag force exerted on the buildings and that is also associated with the local wall shear stress. The concept of an 'exchange' velocity was introduced by Bentham and Britter[29] to describe and model this flow exchange process – an analogue to the 'entrainment' velocity in jets and other shear flows. The flow exchange processes and their modelling are also important for fast-response emergency models where appropriate integral models are derived for the description of the mean flow through and above urban complexes[32]. Experimental as well as computational studies have attempted to estimate the exchange velocity in relevant configurations. Experimental studies include the water-channel experiments by Caton *et al.*[33] aiming to measure the volume flux exchange induced over a 2-D cavity of unity aspect ratio using Particle Tracking Velocimetry (PTV), the flow over regular cube arrays by Barlow *et al.*[34], the variability in the upcoming wind direction over a street-canyon flow by Soulhac *et al.*[35], the effect of atmospheric turbulence on the resulting flow within a unity aspect ratio street canyon by Salizzoni *et al.*[36] as well as the work by Li *et al.*[37] on the flow field within canyons of 3 different aspect ratios and of Princevac *et al.*[38] on the lateral channelling within rectangular arrays of cubical urban obstacles. Computational studies to deduce the corresponding exchange velocity were undertaken using Reynolds-Average Navier-Stokes (RANS) approach[30] as well as Large-Eddy-Simulations (LES)[37]; the latter deduce a temporal average air exchange rate (ACH) for urban street canyons (homogeneous along the length). Analytical developments on the exchange fluxes have been undertaken by Harman *et al.*[39] and Yang and Shao[40]using a resistance-network analysis. Table 1 summarizes these findings of the aforementioned studies with particular attention on the deduced exchange velocities for the different packing densities, providing as well the reference used.

In this paper we present an experimental investigation using Particle Image Velocimetry (PIV) which aims: : (i) to investigate the turbulent boundary layer flow adjusted over two-dimensional rectangular roughness elements, arranged in a building-street canyon geometry, for a range of packing densities; the investigation covers the flow from within the building-street canyons up to a vertical distance reaching the ISL of the adjusted boundary layer profile above, (ii) to determine parameterizations of the adjusted boundary layer and to deduce their variation with a change in the packing density of the roughness elements, and (iii) to report results on the exchange process between the flow within the building-street canyons and the developed boundary flow above and thereby deduce the variation of this exchange process with the packing density of the roughness elements. It is noted that, although the study is motivated in part by a desire to improve our understanding of flows in the urban atmosphere, the underlying flow problem is of more general relevance, and it can also be associated with a range of recent works in the literature, e.g., the DNS of a similar flow by Leonardi *et al.*[21], Orlandi *et al.*[42], or works concerned with the friction over structured surfaces, such as those of Motozawa *et al.*[43] and Ito *et al.*[44].

The paper is structured as follows: the experimental methodology undertaken in this work is presented in Section II, including the experimental apparatus used, the measurements conducted using Particle Image Velocimetry as well as the post-processing analysis performed for the derivation of results relevant to the boundary layer parameterizations and the exchange process. The results from this work are presented and discussed in Section III, which is structured in four sub-sections presenting: (i) the flow phenomenology – flow structure and

velocity field, (ii) the mean boundary layer profiles observed for the geometries of different packing density, (iii) deductions for the atmospheric boundary layer parameterizations such as the surface roughness length and the friction velocity, and finally (iv) deductions for the exchange processes and specifically the exchange velocity with respect to a change in packing density. Finally, our concluding remarks are summarized in Section IV.

Table 1: Summary of studies on and measurements of exchange velocity (reported in non-dimensional form).

Numerical simulations

T. Bentham and R. Britter[29]		λ_p	Exchange velocity (V_{ex}/u_{ref})
Geometry: regular cube arrays;		0.0625	0.037
Measurement: u_{ref} taken at z = 2.5H		0.16	0.0094
		0.44	0.038
D. Hamlyn and R. Britter[30]		λ_p	Exchange velocity (V_{ex}/u_{ref})
Geometry: regular cube arrays;		0.0625	0.0109
Measurement: u_{ref} taken at z = 2.5H		0.16	0.0094
		0.44	0.0032
C.-H. Liu *et al.* [41]		λ_p	Exchange velocity (V_{ex}/u_{ref})
Geometry: street canyon arrays;		0.333	0.03
Measurement: u_{ref} taken as the mean free-surface velocity		0.5	0.05
		0.666	0.04
I. Panagiotou *et al.* [31]		λ_p	Exchange velocity (V_{ex}/u_{ref})
Geometry: real inhomogeneous urban geometry;		0.36	0.0145
with u_{ref} taken at z = 2.5H		0.39	0.0474
(H: average building height, λ_p defined locally)		0.45	0.0131
		0.68	0.0045
Laboratory experiments			
F. Caton *et al.* [33]	*H*/*W*	λ_p	Exchange velocity (V_{ex}/u_{ref})
Geometry: single cavity;	1	0.5	0.026
Measurement: u_{ref} taken as the free-stream velocity			
(no ref. height is reported)			
J. Barlow *et al.* [34]	*H*/*W*	λ_p	Exchange velocity (V_{ex}/u_{ref})
Geometry: regular cube arrays;	2	0.44	0.0011-0.0028
Measurement: u_{ref} taken as the free-stream velocity	1	0.25	0.0019-0.0029
(no ref. height is reported)	0.6	0.14	0.0017-0.0031
	0.25	0.04	0.0018-0.0036
P. Salizzoni *et al.* [36]	*H*/*W*	λ_p	Exchange velocity (V_{ex}/u_{ref})
Geometry: regular street-canyon-like arrays;	1	0.5	0.066-0.078
Measurement: u_{ref} taken as taken as the free-stream velocity			
(no ref. height for U_∞ is reported)			
Analytical work			
Y. Yang and Y. Shao[40]	*H*/*W*	λ_p	Exchange velocity (V_{ex}/u_{ref})
Geometry: regular urban street canyon;	*full range*	*full range*	*f(H/W) based on aerodynamic resistance*
Measurement: u_{ref} taken as the mean free-surface			*network; while also being a function*
velocity			*of other geometrical parameters*

II. EXPERIMENTAL METHODOLOGY

A. Apparatus

1. Water flume

Figure 1 shows the modular water flume (Gunt HM 162 flow channel) that was employed in this study. The channel has a rectangular cross-section with transverse span s = 0.31 m (refer also Figure 2 for flow geometry details) and an overall height of 0.45 m. The total length of the channel was 8.75 m. Nevertheless, in the measurements presented in this paper the total depth of the water flow just upstream of the urban canopy was in the range d = 0.31-0.38 m (indicated in Figure 1). In addition, complete optical access to the channel flow in the flume was guaranteed by glass sidewalls over a length of about 7.5 m of the flume. The modelled geometry is essentially two-dimensional; the urban canopy models (#16 in Figure 1) were situated approximately halfway along the floor of the flume.

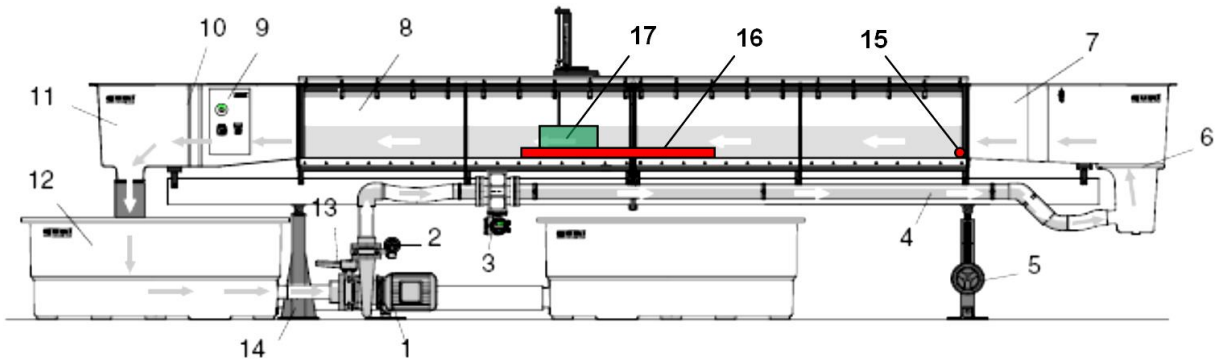

1. Centrifugal pump
2. Shut-off valve hand wheel for flow rate regulation
3. Flow rate meter
4. Pressure line
5. Incline adjustment facility
6. Flow rectifier
7. Intake flow preparation section
8. Modular centre element
9. Switch box
10. Overflow sensor
11. Outflow element
12. Tank
13. Shut-off valve
14. Fixed bearing
15. Trip wire
16. Urban canopy model
17. Measurement area

Figure 1: Water flow channel apparatus.

The intake element (#7 in Figure 1) was modified to contain: (i) a honeycomb section with hole size 6.2 mm and depth 50.8 mm (i.e., about 8 diameters), followed at a distance of 0.61 m by, (ii) a perforated plate with hole diameter 5 mm and 60% open area (or, porosity), followed at a distance of 0.12 m by, (iii) a mesh with spacing 1 by 1 lines per mm and a wire diameter of 0.3 mm. Following this flow preparation arrangement, a trip-wire (#15 in Figure 1) was placed on the floor and the side walls of the flume. The trip-wire was used to establish the starting location of the turbulent boundary layer in the channel. A trip-wire with diameter W_D = 2 mm was used. For this choice of W_D it was asserted that the Reynolds number based on the free stream velocity in the channel U_∞ and wire diameter W_D, i.e., $Re_{WD} = U_\infty W_D/\nu$, was approximately equal to 800, a value that is in line with similar attempts in other studies[18].

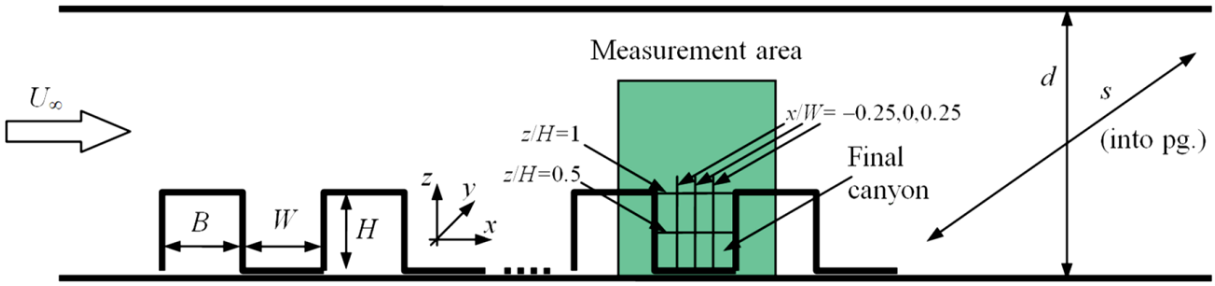

Figure 2: Urban canopy-geometry model.

Mean volumetric flow rates between 0.033 and 0.036 m^3/s were achieved, resulting in bulk velocities (time-averaged volumetric flow rates, averaged over the cross-sectional flow area) upstream of the urban canopy of U_b = 0.28-0.38 m/s. Based on a value of the working fluid kinematic viscosity (ν = 0.9×10^{-6} m^2/s at 25 °C), these velocities correspond to a Reynolds number based on the bulk flow speed U_b and the height of the model buildings H (see Figure 2) of Re_H = 19,000-25,000. It is noted that although this value may be 1-2 orders of magnitude smaller than what is of typical encountered at atmospheric conditions, it is nevertheless high enough to ensure a turbulent flow regime, and that in these conditions the flow is expected to be Reynolds number invariant. Moreover, Meroney *et al.*[45] confirms that for atmospheric flow modeling some further specific similarity criteria, initially prescribed by Hoydysh *et al.*[46] and Snyder[47], are: (i) that the Reynolds number at the canyon cavity needs to exceed 3,400, and (ii) that the roughness Reynolds number should be larger than 2.5. Both of these criteria are satisfied in our series of experiments. Details relating to the channel and flow geometry are summarized in Table 2.

Table 2: Specifications of the flow channel.

Total length	8.75 m
Extent of optical access	7.50 m
Channel cross-section transverse width (s)	0.31 m
Overall channel cross-section height	0.45 m
Water depth upstream of urban canopy model (d)	0.31-0.36 m
Mean employed volumetric flow rates	0.033-0.036 m^3/s
Bulk velocities upstream of the urban canopy (U_b)	0.28-0.38 m/s
Macroscale Reynolds number upstream of the urban canopy (Re_H)	19,000-25,000

2. Upstream boundary layer

The velocity in the channel flow upstream of the urban canopy model, i.e., upstream of the 1st building, was measured with the same PIV system that was used for the rest of the experiments presented in this paper and described below in Section II.B. The result for the vertical profile of the horizontal (axial) velocity at the mid-span (i.e., half-way along the y-direction; see Figure 2) in-between the two vertical sidewalls of the water channel is shown in Figure 3. This profile was generated 0.4 m upstream of the test-model (i.e., upstream of the leading face of the 1st building) in conditions that closely resembled those of the rest of the measurements, with a bulk velocity

U_b of 0.33 m/s. The model building height in all experiments, including this one, is H = 60 mm (see Table 2 for more details). It is an average of 100 instantaneous PIV captures.

Closer inspection of the boundary layer profile that appears at this location gives a 99% velocity thickness of 23.8 mm, a displacement thickness of δ_1 = 6.2 mm and a momentum thickness of δ_2 = 4.8 mm. The shape factor associated with these thicknesses is δ_1/δ_2 = 1.3, which is typical of turbulent boundary layers. In addition, the friction velocity normalized by the bulk velocity u^*/U_b was estimated from a plot of u_x as a function of the natural logarithm of z (i.e., a logarithmic version of Figure 3a, shown as Figure 3b) and was found to be 0.186.

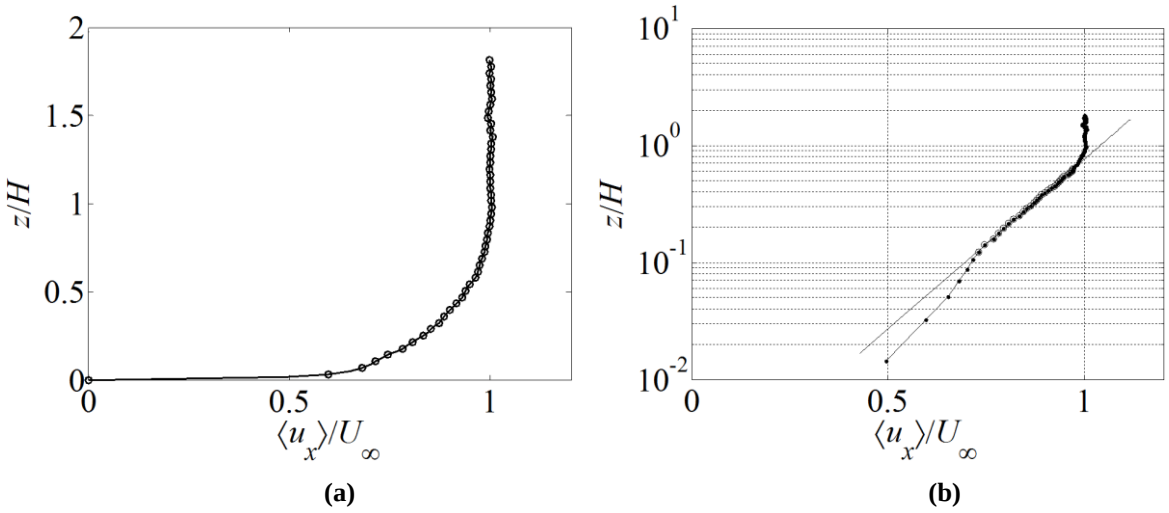

Figure 3: Measured boundary layer profile upstream of the urban canopy/geometry model in: (a) linear and (b) semi-logarithmic axes.

3. Urban canopy models

Each urban canopy model used in the current study (illustrated schematically in Figure 2) consisted of 6 buildings forming 5 canyons in an essentially two-dimensional geometry. The buildings and resulting canyons were positioned perpendicularly to the flow direction; each building was represented by placing a block of wood with square cross-section on the flume floor, and across the whole width of the channel. As such, the total spanwise length of all buildings L was equal to the span of the channel $L = s$ = 0.31 m (see Table 2).Denoting the height of the blocks with H = 0.06 m and their breadth with B = 0.06 m, the height-to-breadth ratio H/B was kept equal to 1 (see Figure 2). The same blocks were used for all investigated canopy models. Given that in urban geometries the ratio H/B can range from 0.25 to 2, a value of unity was chosen as representative of a typical urban environment. This value is also used by other investigators[33,34]. Further, the slenderness ratio of the buildings (length L over height H, L/H) was also kept constant across all investigated geometries with a value of L/H = 5.2.

Repeated canyons in-between buildings were formed by placing the buildings at a regular spacing. The wooden blocks were placed at equal and regular distances W (as in Figure 2), thus forming a homogeneous geometry with a constant packing density value $\lambda_p = B/(B+W)$. Each canyon comprised two flat horizontal surfaces at an elevated height H above the flume floor from consecutive building roofs, and a cavity located between them consisting of two vertical surfaces from the building walls and the horizontal flume floor.

Measurements were made at the spanwise (y-direction) symmetry plane (i.e at y=L/2), in a vertical plane half-

way between the two vertical sidewalls of the flume. The thickness of the side-wall boundary layers was ensured to be small enough (compared to the span L), reassuring thus that any sidewall effects were negligible at the measurement location and the set of measurements was conducted in the 5th canyon downstream, that is, between the 5th and 6th building (as indicated in Figure 2). This was done since in previous studies[18], it was shown that, for flow inside and above an array of two-dimensional idealized street canyons, the flow becomes vertically homogenous after a fetch of 3 to 4 canyons. Table 3 summarizes the various investigated urban canopy geometries.

Table 3: The set of 2-D urban street-canyon geometries in the experimental investigation.

Case Study	H [m]	D [m]	W [m]	d [m]	s [m]	U_b [m/s]	H/B [–]	$\lambda_p = B/(B+W)$ [–]	H/d [–]	$Re_H = U_bH/\nu$ [–]
1 (‘dense’)	0.06	0.06	0.030	0.36	0.31	0.30	1.0	0.67	0.17	20,000
2	0.06	0.06	0.050	0.36	0.31	0.28	1.0	0.55	0.17	19,000
3	0.06	0.06	0.060	0.36	0.31	0.29	1.0	0.50	0.17	20,000
4	0.06	0.06	0.075	0.35	0.31	0.32	1.0	0.44	0.17	21,000
5	0.06	0.06	0.090	0.32	0.31	0.35	1.0	0.40	0.19	24,000
6	0.06	0.06	0.100	0.35	0.31	0.30	1.0	0.38	0.17	20,000
7	0.06	0.06	0.120	0.31	0.31	0.38	1.0	0.33	0.19	25,000
8 (‘sparse’)	0.06	0.06	0.140	0.36	0.31	0.28	1.0	0.30	0.17	19,000

B. PIV measurements

A *LaVision* Flow Master Particle Image Velocimetry (PIV) system was used to measure the flow velocity in the interrogation measurement area illustrated in Figure 2. The measured field of view extends up to a distance of 1.5*H* from the rooftop level reaching a total height from the ground of 2.5*H*. Standard hollow glass sphere tracer particles of diameter 9-13 μm were seeded into water, as in previous PIV studies in liquid flows. The particles occupied an area approximately 2-3 pixels in diameter on the generated images. A laser sheet of mean thickness 0.10 mm over the measurement plane was used to illuminate the flow field. The size of the field of view was approximately 0.15 × 0.15 m. The laser was a 125 mJ frequency-doubled Nd:YAG at 532 nm (model Nano L 125-15 supplied by Litron Lasers). Measurements were performed at 7 Hz.

The camera was a 14-bit LaVision Imager Pro X 4M CCD with 2048 × 2048 pixels of size 7.4 × 7.4 nm. The resulting pixel resolution was 0.07 mm per pixel. The time interval between the consecutive images in a PIV image pair was offset according to the mean bulk velocity (estimated from the known mean volumetric flow rate and flow cross-sectional area) and the size of the PIV window to achieve a displacement of 3 to 10 pixels. In this work, square 64 × 64 pixel PIV windows were used with 50% overlap. Before overlapping, the PIV spatial resolution was 4.7 mm, however, the overlapping procedure allows the reporting of velocities over spatial distances half of the PIV resolution, though with increased uncertainty. For certain conditions (e.g., the symmetric Case Study 3 with λ_p = 0.5) more than one measurement was made, for measurement quality checks and in order to reduce measurement errors and ascertain the repeatability of the experiments.

C. Post-processing and analysis of results

From each consecutive image pair a single instantaneous velocity field was generated by using LaVision's DaVis software. The statistical mean and root-mean-square (rms) of the fluctuations of the two velocity components were compiled from the instantaneous images ($u_{x,i}$: horizontal; $u_{z,i}$: vertical at time instant 'i'), from:

$$\overline{U_x} = \frac{1}{n}\sum_{i=1}^{n} u_{x,i} \; ; \quad \overline{U_z} = \frac{1}{n}\sum_{i=1}^{n} u_{z,i} \tag{2}$$

$$U_{x,\mathrm{rms}} = \sqrt{\frac{1}{n-1}\sum_{i=1}^{n}\left(u_{x,i} - \overline{U_x}\right)^2} \; ; \quad U_{z,\mathrm{rms}} = \sqrt{\frac{1}{n-1}\sum_{i=1}^{n}\left(u_{z,i} - \overline{U_z}\right)^2} \tag{3}$$

This also allowed the evaluation of the local mean velocity and turbulent kinetic energy in 2-D,

$$\overline{U} = \sqrt{\overline{U_x}^2 + \overline{U_z}^2} \tag{4}$$

$$k_{2\mathrm{D}} = \frac{1}{2}\left(U_{x,\mathrm{rms}}{}^2 + U_{z,\mathrm{rms}}{}^2\right) \tag{5}$$

as well as the Reynolds stresses RS_{xz}, which were calculated from,

$$RS_{xz} = \left\langle u_x{}' u_z{}' \right\rangle = \frac{1}{n}\sum_{i=1}^{n}\left(u_{x,i} - \overline{U_x}\right)\left(u_{z,i} - \overline{U_z}\right) \tag{6}$$

In addition, the analysis required the estimation of an 'exchange' velocity V_{ex}, containing information on the underlying physical processes of in-canyon ventilation. This velocity was defined in this work as the total mean flux out of (or into) the canyon, evaluated at rooftop level height $z = H$, divided by the distance between the buildings W, with a non-dimensional description also used in which V_{ex} is divided by the bulk velocity U_{b},

$$V_{\mathrm{ex}} = \frac{1}{2W}\int_{-W/2}^{+W/2}\left|\overline{U_z}(z = H)\right|\mathrm{d}x \; ; \quad \tilde{V}_{\mathrm{ex}} = \frac{V_{\mathrm{ex}}}{U_{\mathrm{b}}} \tag{7}$$

Similarly, the same integral was evaluated at two vertical levels inside the canyon $z = z_{\mathrm{vc}}$, specifically, at the height of the recirculation-cell core $z = Z_{\mathrm{vc}}$, and mid-height $z = H/2$), leading to an equivalent velocity scale,

$$V_{\mathrm{vc}} = \frac{1}{2W}\int_{-W/2}^{+W/2}\left|\overline{U_z}(z = z_{\mathrm{vc}})\right|\mathrm{d}x \; ; \quad \tilde{V}_{\mathrm{vc}} = \frac{V_{\mathrm{vc}}}{U_{\mathrm{b}}} \tag{8}$$

Finally, it will be stated in Section III.C that the standard deviation of u_z, σ_z, was in the range of 0.24 to 0.94 of its mean value at the rooftop level. Given the 35 instantaneous samples of u_z from which the time-averaged value of u_z is evaluated, this results in a statistical standard error in the mean reported values of $\overline{U_z}$ (which is

given by σ_z/sqrt(n); with n the number of samples used) of 4% to 15%.

III. RESULTS AND DISCUSSION

A. Phenomenology: Flow structure and velocity field

The qualitative mean flow structure and its variation across the different packing densities can be observed by producing visualizations of the mean flow streamlines from the directly measured flow velocity vectors. Figure 4 depicts the observed time-averaged velocity vector fields and flow streamlines over the range of the investigated test cases in this paper. In all cases, the mean flow within the canyon cavity consists of a dominant recirculation cell, whose basic form appears to persist throughout the investigated range of canyon geometries, and a shear layer developing and extending over the canyon cavity centred at the rooftop level. Overall, it is observed that the recirculation velocities are much weaker than the velocities observed above the rooftop level. The cell appears to adjust to the geometrical packing density change, keeping a (close to) symmetric form in the range of geometries with λ_p ranging within $0.44 < \lambda_p < 0.55$ (or with $\lambda_p \approx 0.5 \pm 10\%$), but then shifting to a clearly asymmetric form (with its centre displaced both vertically and horizontally) as the geometry deviates from the square cavity (i.e., deviating from $\lambda_p = 0.5$, or $H/W = 1$). The recirculation cell is bounded by a flow of strong shear that reattaches at the leeward (downstream; on the right) building of the canyon. In the two extreme geometries (narrowest and widest) the symmetry of the flow structure within the canyon breaks and the main recirculation cell centre elevates to the upper part of the canyon cavity. In addition, in the case of the wider cavities ($\lambda_p < 0.5$) the core of the main recirculation cell is also shifted horizontally towards the leeward side.

The vertical location of the recirculation cell cores shown in Figure 4 across the investigated cases is depicted in Figure 5a, with the symmetric (centre point) location in the canyon cavity corresponding to $x/W = 0$ and $z/H = 0.5$. It is interesting to note the initiation of secondary flows in the extreme case geometries (i.e., the narrowest and widest canyon cavities). In the narrowest canyon case, a secondary flow structure appears below the main recirculation cell – to the leeward side, while in the widest canyon case a secondary flow structure is initiated in the windward bottom corner of the canyon. These observations are consistent with those by Oke[48,49] and revisited by Harman *et al.*[39]. Further, Figure 5b shows the variation of the dimensionless (with respect to U_b and W) bulk net flux, V_{vc}, at the level of the internal canyon recirculation-cell core, as a function of the geometric packing density variation; at the "narrowest" case ($\lambda_p = 0.67$) the two location-points reflect the appearance of a secondary cell near the bottom. This V_{vc} attribute reflects the capacity of the canyon to circulate and mix any scalar (be it pollutant or heat) within the volume of the canyon. The maximum net flux is observed in the urban canyon geometries of $\lambda_p = 0.5$, or $H/W = 1$, regardless of the capacity of the canyon for eventual removal of the scalar out of the canyon (through its rooftop level at $z = H$).

Returning to Figure 4, it is also obvious that all flows observed in the investigated range of test cases are within the skimming-flow regime. Specifically, the observed recirculation cells in all of our test cases occupy the entire lateral canyon-cavity area. This observation is consistent with the classification of flow regimes suggested by Oke[48,49] based on the canyon aspect ratio: specifically it is suggested that for the 'ventilation' regime to be observed, a cavity with an aspect ratio of $H/W < 1/3$ (corresponding to $\lambda_p < 0.25$) is required, which is outside the range of our tested geometries. In our test cases the skimming-flow regime is found to persist down to the lowest canyon aspect ratio of $H/W = 0.43$ (corresponding to packing density of $\lambda_p \sim 0.3$). Beyond Oke's flow regime classification, we also observe for the case of $H/W = 2$ ($\lambda_p = 0.67$) an 'elevated' skimming-flow regime, in which

secondary flows are initiated below the main recirculation cell, in a region occupying the bottom 1/3 of the canyon height (see Case 1 in Figure 4). This may be an important feature to account for when considering the flow and dispersion processes in real urban geometries, where such canyon aspect ratios are frequently encountered, particularly in European urban settings.

As a final point of interest with regards to the overall qualitative flow features, it is noted that the time-averaged flow maps shown in Figure 4 cannot convey any unsteady flow effects that were, in fact, observed on inspecting the instantaneous 2-D vector field data. These effects include a fluctuating translation of the vortex core both vertically and horizontally within the canyon cavity. Therefore, it is concluded that although the maps shown in Figure 4 indicate a strong mean flow phenomenology featuring a large-scale vortical structure (and possibly secondary ones) as stated above, these do not suggest that this flow structure is steady.

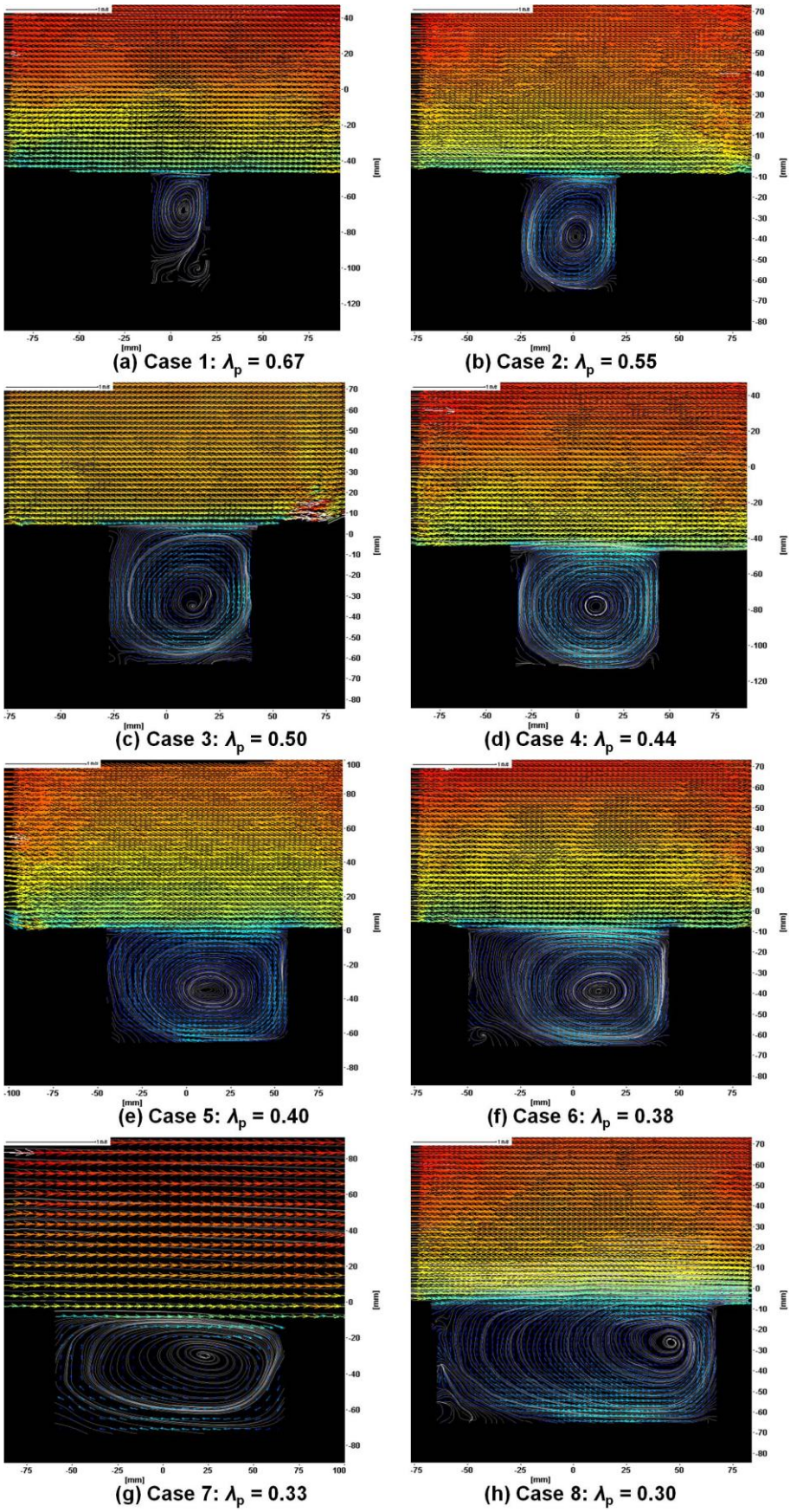

Figure 4: The flow velocity fields and streamlines obtained using PIV measurements in the range of test cases conducted.

B. Mean flow velocity profiles and turbulence

1. Mean flow

The measured vertical profiles of the mean horizontal flow velocity component, u_x, in and above the street canyon are shown in Figure 6 of all test cases (i.e., for all λ_p). Profiles are shown at three different horizontal positions across the width of the canyon, specifically at: (i) $x = -W/4$, (ii) $x = 0$, (iii) $x = +W/4$, where $x = 0$ is the central position at mid-width and W is the width of the canyon. The profiles are normalized over the value of the horizontal velocity u_x at a height $z = 2.5H$ at the corresponding x-position where the profiles were generated; e.g., $\langle u_x(x/W=0;z=2.5H)\rangle$ for the central position. The vertical profiles at all three positions display a reverse flow near the ground level for all canyon aspect ratios, as would be expected due to the presence of a recirculation cell.

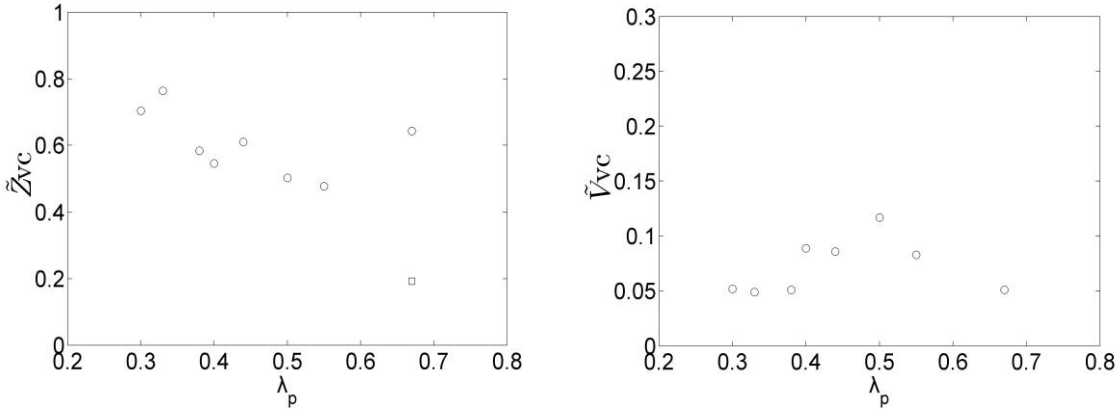

Figure 5: (a) The dimensionless (with respect to H) vertical position (Z_{vc}) of the internal canyon recirculation cell core. (b) The dimensionless (with respect to U_b and W) net bulk flux (V_{vc}), evaluated from Equation (8).

Moreover, the vertical profiles of u_x in each plot appear similar, with the exception of the narrowest canyon (that is, $H/W = 2$; $\lambda_p = 0.67$) that exhibits the elevated recirculation cell that was also displayed in Figure 5 (Case 1). It is noted that there is no discernible difference in the qualitative flow behaviour, or vertical profile shape, across the three different lateral positions in Figure 6. An average of the profiles of u_x over the three different x-positions shown may be obtained for each λ_p case. These spatial averages are shown in Figure 6d, from which an average effect of the packing density on the horizontal velocity can be deduced.

An examination of the flow above the canyon rooftop level reveals a horizontal velocity (or speed) profile whose steepness varies with vertical height, indicating that an adjustment of the flow is taking place from the canyon region. The different adjustments of the same approaching boundary layer can be related to the different packing density of the urban geometry in each case.

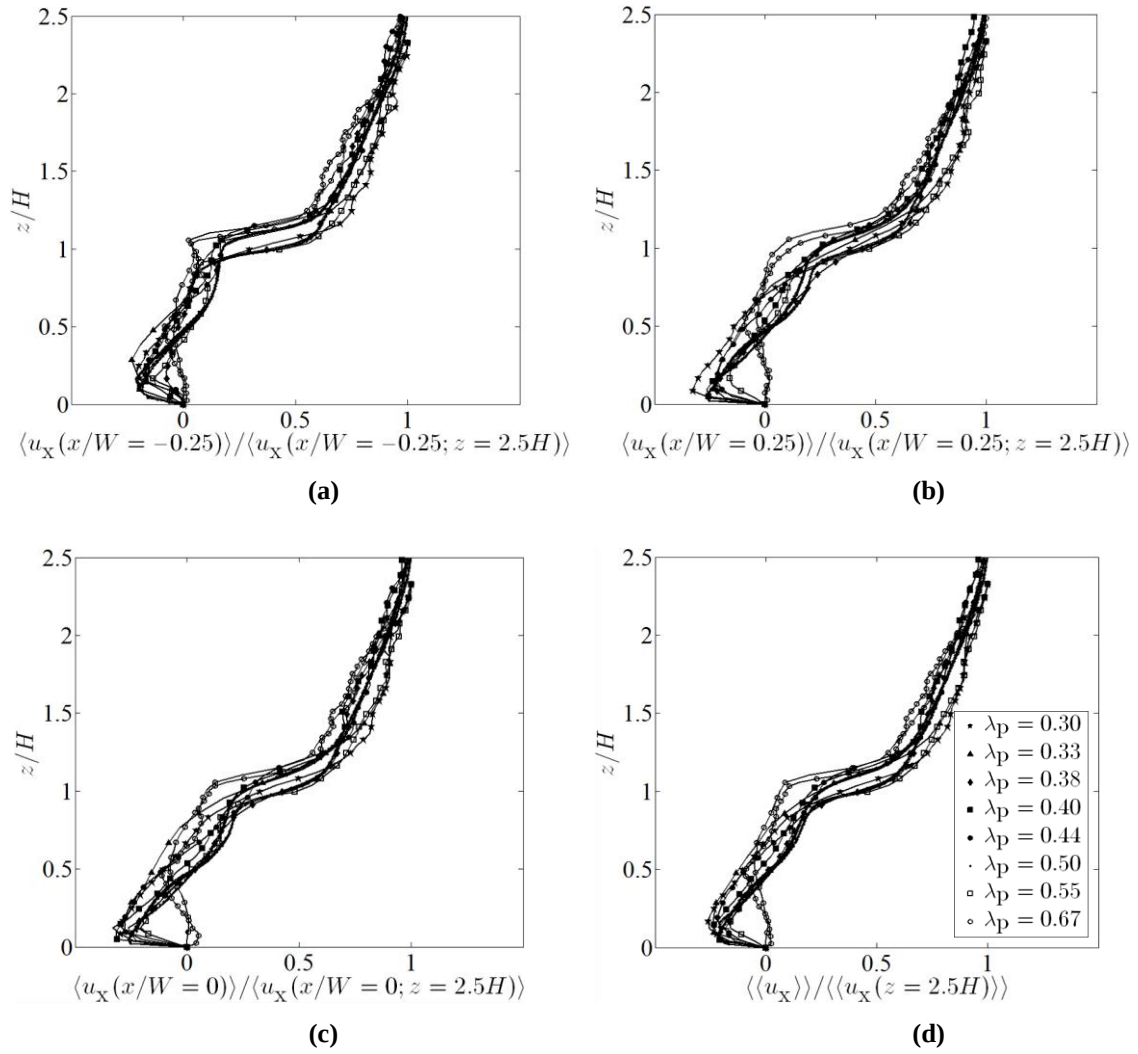

Figure 6: Vertical mean velocity profiles in the broader street canyon normalized over the mean velocity at the height z/H = 2.5. Showing profiles at 3 different horizontal positions: (a) x/W = -0.25, (b) x/W = +0.25, and (c) x/W = 0; along with (d) average vertical mean velocity profiles, averaged over the three horizontal positions shown in (a-c) and depicted at the half-width.

What can be considered an appropriate reference velocity for use in the normalization of these profiles to establish similarity is subject to discussion in the literature[7,15,22,23]. The use of a reference velocity relatively far away from the cavity (e.g., at $z = 2.5H$) contains almost no information on: (i) the impact of the ground surface geometry on the flow, and (ii) the resulting shear layer and its interaction with the recirculation flow in the cavity below. On the other hand, a reference velocity lower down (for instance, referenced at the rooftop level, i.e., at height $z = H$) will be strongly affected by the underlying shear layer, and will contain substantial information on both the roughness sublayer and the inertial sublayer. The extent of the roughness sublayer and hence the onset of the inertial layer are related to the turbulence characteristics. Depending on which part of the flow is to be addressed and analysed, the appropriate reference should be selected.

Examining the part of the flow inside the canyon cavity, where it would correspond to all the civilian and other urban activities taking place, Figure 7 presents the vertical profiles of the horizontal velocity u_x at the same three locations across the canyon width as those used in Figure 6 focusing within the canyon region, i.e., $z \leq H$. The

vertical coordinate is scaled with the building height H, and the measurement data are normalized by $\langle u_x(z=H)\rangle$, which is the value of the mean wind velocity at $z = H$. This choice for the normalization parameter was primarily determined by the availability of such measurements for most compared datasets. Nevertheless, as will be shown below, this normalization may not necessarily be optimal for presenting velocity data from different laboratory and field experiments. The figure shows a larger variation across the different cases of λ_p than what may have been expected, since the selected reference normalization velocity in this case does contain information on the flow-geometry interaction and such normalization may have smoothened up the differences. In fact, it turns out that the horizontal velocities at the rooftop level are usually significantly smaller compared to the average velocities within the canyon, and normalization over such velocity can yield enlarged differences due to this sensitivity, rather than reflecting a true impact of the geometry on the profiles.

Overall, our findings in terms of the mean velocity profiles can be summarized as follows. The flow above the urban canopy follows in all cases a logarithmic-like profile, while with respect to the flow structure inside the canopy, two types of velocity profiles can be distinguished: over a wide range of canyons, a mean wind velocity reversal is observed (reflecting a recirculation cell), whereas for the most dense/packed geometry (λ_p = 0.67) the flow reversal appears shifted upwards (up to 1/3 of the canyon height) due to the presence of a secondary flow at the bottom corners of the canyon resulting into a greater region of near-zero velocities. These observations are agreement with the wind-tunnel experiments by Kastner-Klein *et al.*[23].

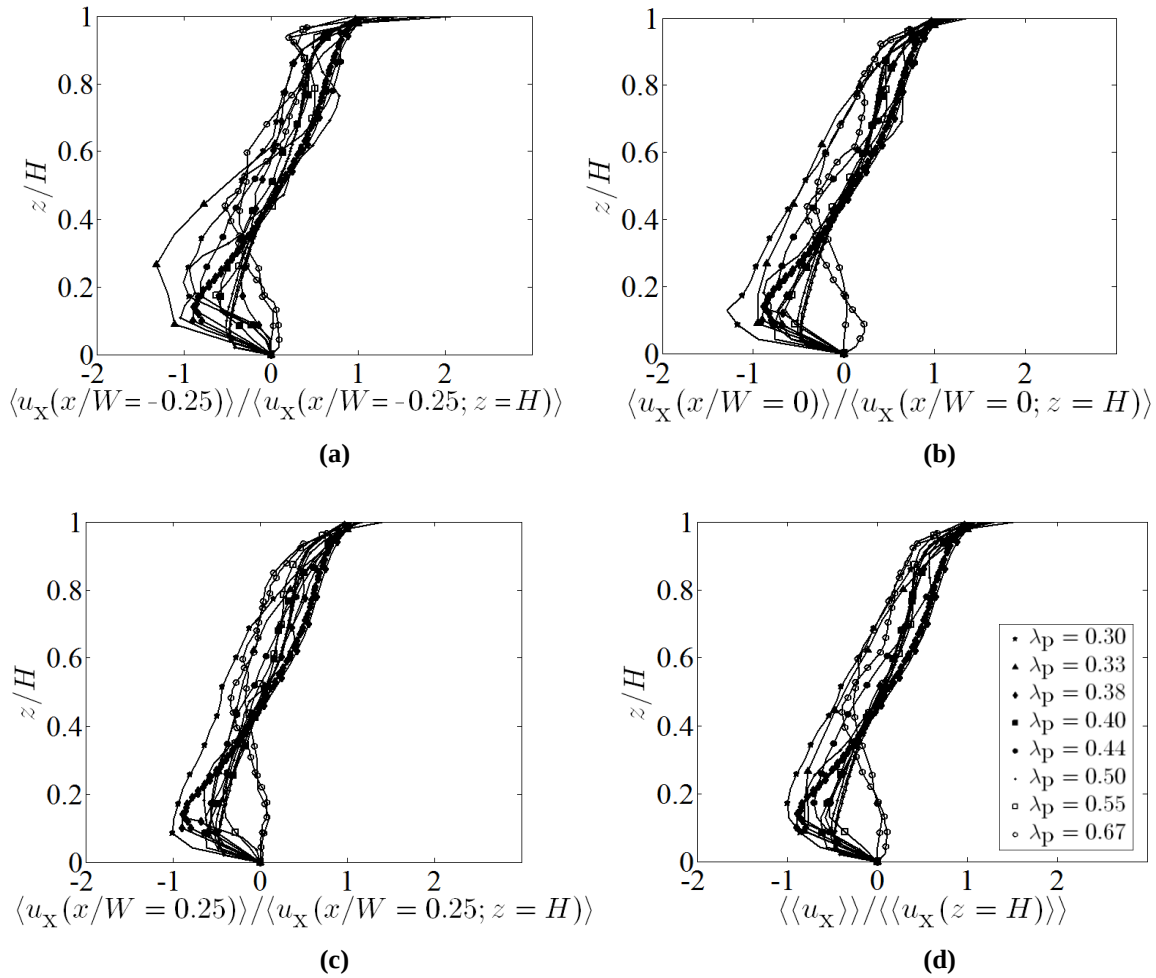

Figure 7: Vertical mean velocity profiles in the core of the canyon normalized over the mean velocity at the rooftop level height $z/H = 1$. Showing profiles at 3 different horizontal positions: (a) $x/W = -0.25$, (b) $x/W = +0.25$, and (c) $x/W = 0$; along with (d) average vertical mean velocity profiles, averaged over the three horizontal positions shown in (a-c) and depicted at the half-width.

2. Turbulence characteristics

Turbulence quantities were investigated by examining vertical profiles of the Reynolds stresses (extending from the ground surface up to $z = 2.5H$), as well as horizontal profiles at the rooftop level. Reynolds stresses (RS), which represent essentially the vertical transport of horizontal momentum due to turbulence solely, is a measure of the drag force per unit area (or surface shear stress) that the canyons exert on the upper free flow, and it can be associated with a friction velocity through $u^* = \sqrt{[\tau_w/(\rho \overline{u_x' u_z'})]}$. Turbulence characteristics at the rooftop level are interesting in the context of pollution escape/removal from the canyon, as well as the removal of other scalars (e.g., relating to heat and thermal comfort).

Figure 8 shows the vertical profiles of the Reynolds stress (RS), $RS_{xz} = \langle u_x' u_z' \rangle$, obtained by a spatial average of the vertical profiles at three lateral positions (at mid-width, quarter-width and three quarter-widths of the canyon) normalized by the (square of the) average bulk flow velocity, U_b. For all the geometries, the RS is insignificant (near-zero) within the canyon cavity. The RS increases (in absolute value) from the rooftop level (at the average zero plane displacement height, $z \approx H$) upwards, from a small value to a maximum, and then diminishes again. This variation reflects the fact that the turbulence levels gradually increase away from the wall in the roughness sublayer and within the shear layer that arises from the rooftops, while further away, in the inertial sublayer, the turbulence decays and becomes less aware of the wall. The RS_{xz} profiles reveal characteristic features of the roughness sublayer (RSL) and their peak demarks, or is representative of, the transition from the roughness to the inertial sublayer. In attempting to connect our laboratory observations with the fields expected in a street canyon of a real city, it is important to address the horizontal inhomogeneity of the flow in the RSL, and therefore, to analyze spatially averaged profiles[14, 23]. However, the importance or relevance of spatially averaged profiles may be questionable for urban street-canyon configurations, at least if they are characterized by skimming flow regimes[50,51]. Consequently our analysis was aimed at the description of individual profiles.

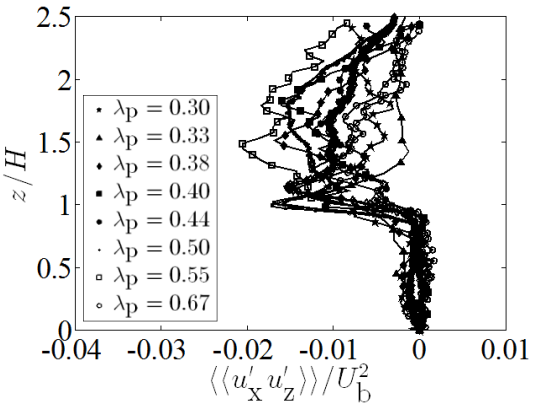

Figure 8: Vertical Reynolds stress profiles, averaged over the horizontal positions at $x/W = -0.25$, 0 and +0.25.

Turbulence characteristics at the rooftop level are interesting in the context of pollution escape from the canyon as they are the only means of momentum transport in the outer region above the canyon. Figure 9a shows the variation of the spatially-averaged Reynolds stress (across the horizontal plane) at the rooftop level against the packing density of the urban geometries. The plot shows a clear RS variability with the packing density of the geometry, with sparse to medium packing densities exhibiting relatively high values of RS, and with the RS values decreasing drastically (more than ~50%) for packing densities above $\lambda_p = 0.5$.

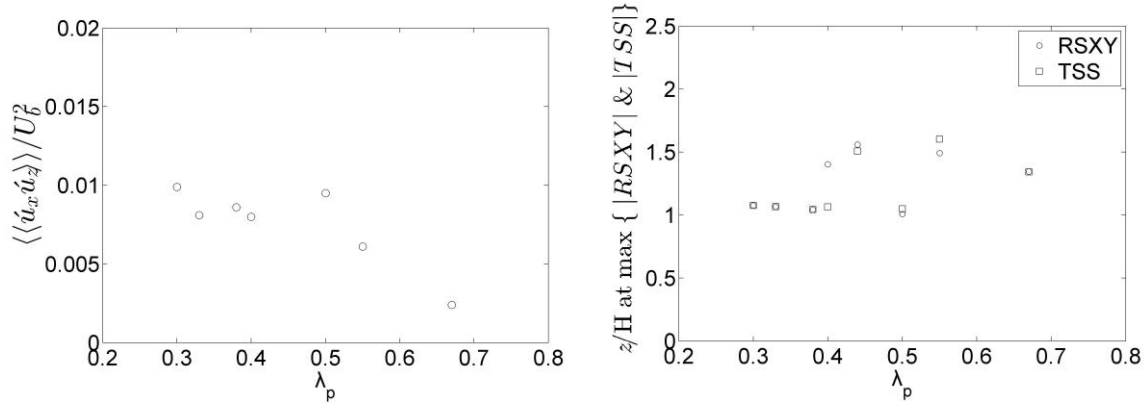

(a) **(b)**

Figure 9: (a) Averaged Reynolds stress RS_{xy} at the rooftop level ($z/H = 1$) over the entire horizontal span, for the different geometries/packing densities. (b) Normalized height at which maximum stress occurs for each packing density geometry, using as indicator the Reynolds Stress maximum (denoted as RSXY) and the Total Shear Stress (denoted as TSS) .

This set of experimental measurements enables us to track the thickness of the roughness sublayer (RSL) and its variation with packing density. Specifically, the maximum value of the shear stress can be used to denote the extent of the RSL, the height of which does not necessarily coincide with the canopy layer (or the roughness-element height). As indicators of the maximum shear stress, the Reynolds stress (RS_{xy}) as well as the total shear stress (TSS) can be used. As already noted, the RSL is composed of the canopy layer, which is demarcated by the rooftop level, and the shear layer forming right above the rooftop level. It is observed in our results, in Figure 9b, that the extent of the RSL thickness depends on the packing density, and ranges from ~1.0H (min) at $\lambda_p = 0.3$ to 1.6H (max) at $\lambda_p = 0.7$.When the packing density is low (below 0.4), the shear layer above the canopy is very thin and essentially the inertial layer lies almost just above the canyon cavity enabling higher exchange of momentum flux. When the packing density increases above 0.4, the shear layer grows thicker, extending up to a further distance of 0.6H (at $\lambda_p = 0.7$) above the canopy level, and longer, essentially almost isolating the cavity from the inertial sublayer, and diminishing any momentum flux exchange at the rooftop level in the canyon. For the sake of comparison, we note that Rotach[25,26] observed the RS_{xz} maxima in field measurements in an urban street canyon of $H/W \approx 1$ at a height $z = 2H$, while Oikawa and Meng[52] – also in field measurements – observed RS_{xz} profiles that peaked at a level of 1.5H. The RS_{xz} values can also provide estimates for the friction velocity u^* [25,26]; this will be considered in the proceeding section.

C. Urban scale considerations: Deduction of aerodynamic parameters of the urban boundary layer

There is a number of ways to deduce friction velocity from the experimental measurements. One way is by examining the vertical profiles of the horizontal velocity above the rooftop level at the mid-width of the canyon (Figure 6c), and confirming the logarithmic-like variation. By assuming neutral or adiabatic conditions and a boundary layer flow profile conforming to the Monin-Obukhov similarity theory described by Eq. (1), i.e., $u(z) = (u^*/\kappa)\ \ln[(z - d_0)/z_0]$, a friction velocity u^* was deduced, which best fitted the data. In addition, the values of surface roughness length z_0 and displacement thickness d_0 were extracted according to considerations made in Kastner-Klein and Rotach[24]; it is noted that only the subset of measurement points that satisfied $z - d_0 > d_0$ were selected for drawing the linear-log profile on the experimental measurements.

The friction velocity was also deduced by alternative approaches; onother approach is by using the maximum value of the measured Reynolds (or Total shear stress) stress in the vertical profile at the mid-width, from which a friction velocity was deduced using $u^* = \sqrt{[\tau_w/(\rho u_x' u_z')]}$. Figure 10 shows all the deduced values of friction velocity for the corresponding H/W ratios (or packing density ratios, λ_p) using the various methods. The variability between the different methods is minimal (a few percentages) at medium geometries ($\lambda_p = 0.44$) and grows for the sparser geometries (to 20%). It was observed that the maximum friction velocities are obtained for the medium-packed geometries while smaller values (approximately by 1/3) are observed for the most dense and sparse geometries. This variation seems to be consistent with the variation of the shear layer extent; for the narrowest geometries the interfacial area of shear is relatively smaller, the momentum exchange is smaller while the shear layer, as well, cannot grow substantially before the next rooftop appears. In the most sparse geometries, despite that the interfacial area of shear is larger, the actual mean velocity shear is smaller.

It is argued that a vertical lengthscale which can be representative of the extent of the roughness sublayer may be appropriate for non-dimensionalisation and the determination of similarity profiles and scalings, as it marks the start of the inertial sublayer. Figure 9a shows the deduced vertical heights (normalized over the building height H) at which the maximum Reynolds stress occurs for each packing density; ranged from 1.0 in the lower packing density ratios to approximately 1.6 in the medium packing densities ($\lambda_p \sim 0.5 \pm 10\%$) – with the exception of the point with the square canyon (or $\lambda_p \sim 0.5$) where the height of the maximum stress (either Reynolds or total shear stress) was actually found to be considerably lower that adjacent points, at $z/H \approx 1$.

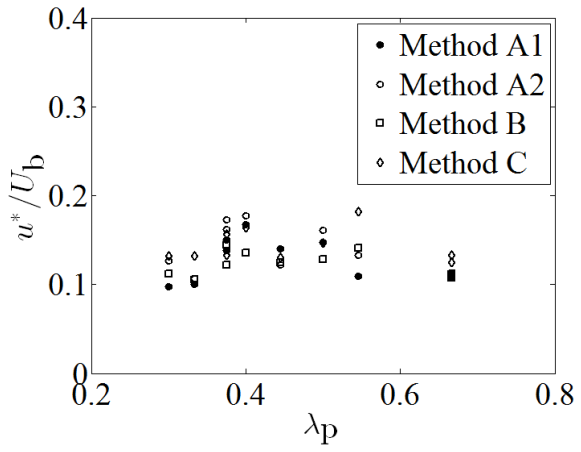

Figure 10: Variation of the friction velocity deduced from the PIV measurements with the packing density of

urban geometry. Method A1: from $U = f(\ln(y))$ gradient with d_0 imposed from Kastner-Klein and Rotach[23]. Method A2: from $U = f(\ln(y))$ intercept '2' with z_0 imposed from Kastner-Klein and Rotach[23]. Method B: from $max\{|RS_{xz}^{1/2}|\} = max\{|\langle u_x' u_z' \rangle^{1/2}|\}$. Method C: from maximum total shear stress as $max\{|TSS_{\max}^{1/2}|\}$.

It was discussed earlier (with reference to Figure 8) that a characteristic feature of the RSL is an increase in the absolute value of Reynolds stress (from essentially zero within the canyon up to the rooftop level) to a maximum value (as already reported earlier to range from H to $1.6H$). Similar Reynolds stress profiles to those obtained in our laboratory measurements were observed by Oikawa and Meng[52] in field measurements at the outer edge of a suburban area (prevailing winds coming from the direction of the built-up area). In that work, the profiles peaked at a level 1.5 times the average building height H. The friction velocity u^* was determined from flux measurements at $2.6H$, a height that they considered to be above the RSL, with this u^* value being about 7% lower than the peak value. Rotach[26] in similar field measurements found a value for the transition of RSL to ISL of $2H$.

In a similar way to the deduction of the friction velocity u^* using Eq. (1), the aerodynamic surface roughness length z_0 and zero-plane displacement height d_0 were also deduced for each test case geometry using the methodology suggested by Kastner-Klein and Rotach[23]. These are plotted as a function of the packing density in Figure 11. As this work is partly motivated by an interest in understanding also real urban flows, we also present in Figure 11 altogether the results from relevant but distinct types of cases currently available in literature: (i) the idealized homogeneous canyon arrays under controlled laboratory conditions (of this presented work); (ii) the heterogeneous canyon case under controlled laboratory[23] (iii) the case of real field data (that includes natural wind variability) using morphometric methods[7], and (iv) the homogeneous cubical building arrays[51] for the zero-plane displacement height d_0 .We note that the figure is not intended to be a comparison of precisely equivalent values, but contextual, i.e., to provide a context of how, building on the idealized fundamental canyon-array problem (presented in this work), corresponding results gradually evolve towards those obtained in the realm of the field. This contextual plot shows that cases which include heterogeneity and natural wind variability yield a higher surface roughness length $z_{0,}$ ranging from 2.5 to 10 times higher than that yielded in idealized homogeneous canyons cases – depending on the packing density as shown in Figure 11a. For the yielded zero-plane displacement thickness d_0, it is observed from Figure 11b that for the idealised homogeneous roughness elements (denoted in the Figure 11b as "present study"), there is a gradual increase of the displacement height with increasing packing density. As expected, the normalized displacement height approaches unity at the highest packing densities (where the collection of roughness elements corresponds almost to an elevated floor/ground), whereas at the lowest packing densities, the displacement thickness has its lowest values. In this figure plot (Figure 11b), there is also a further dataset available, by Macdonald[13], with an idealised geometry comprised of homogeneous regular cubical arrays. The comparison in this plot with other datasets is also contextual; the trends observed in the variation of zero-plane displacement thickness with the packing density of the roughness elements are similar for the different cases– with the smallest values corresponding to the idealised 2-D canyon array (denoted as "present study") and the highest values corresponding to the field, i.e., real heterogeneous urban area under real wind field conditions (denoted as "Britter & Hanna (2003)" in the plot).

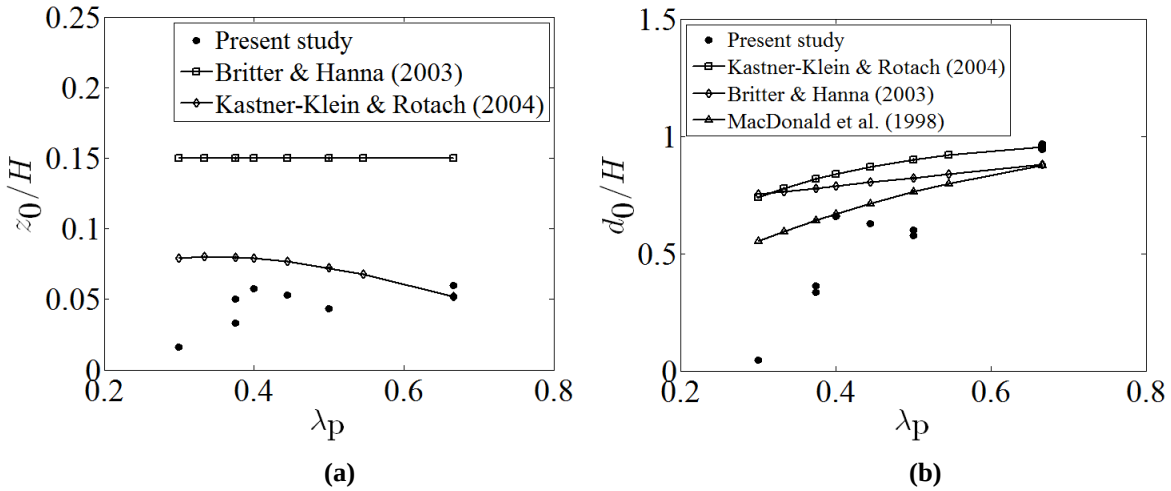

Figure 11: (a) The deduced variation of the surface roughness length z_0 with the geometric packing density, (b) Variation of the zero-plane displacement thickness/height d_0 with the geometric packing density, for the idealized, homogeneous 2-D rectangular-canyon-like roughness elements and contextual comparison with: the heterogeneous canyon case in a modelled real urban area under controlled laboratory conditions by Kastner-Klein *et al.*[23]; the case of real field data (including natural wind variability) using morphometric methods by Britter and Hanna[7]; the homogeneous cubical building arrays by McDonald[51] for the zero-plane displacement height d_0.

D. Street scale: Exchange processes between the in-canopy and above-canopy flows

Figure 12 shows the horizontal profiles of the mean vertical velocity at: (a) the mid-height of the canyon, $z = H/2$, and (b) at the rooftop level, normalized in both cases over the bulk velocity U_b as defined in Section II. The profiles show a positive (upwards) velocity at the windward side and a negative (downward) velocity at leeward side within the canyon, which result directly from the recirculating cell (as seen previously in Figure 4). In the narrower canyons ($H/W \leq 6/9$) the profiles are symmetric, with respect to the mid-width, i.e., the areas of inflow and outflow are equal, with the zero-velocity crossing point found at $x/W = 0.1 \pm 0.05$ (with its centre at $x/W = 0$) in all cases, except the widest canyon where it is found at $x \approx 0.3W$. These horizontal profiles of vertical velocity become increasingly asymmetric with increasing canyon width ($H/W > 6/9$).

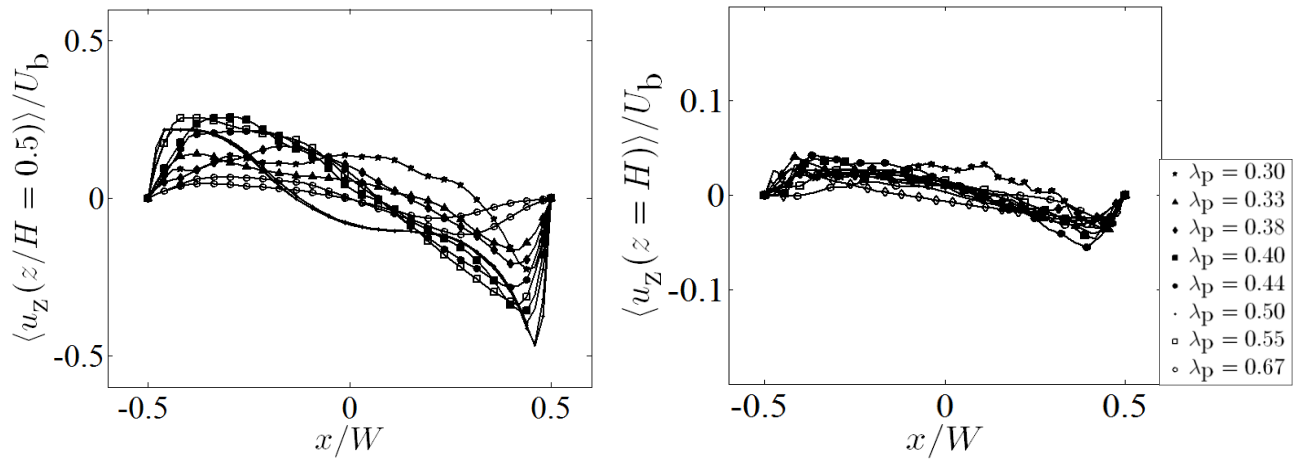

(a) **(b)**

Figure 12: (a) Horizontal profiles of the vertical velocity at the mid-height level of the modelled street-canyon, for all tested geometric packing densities. (b) Horizontal profiles of the vertical velocity at the rooftop of the modelled street-canyon, for all tested geometric packing densities.

The exchanged flux may be a result either due to a mean flux exchange or a turbulent exchange. An exchange velocity can be deduced from the magnitude of the exchanged volume flux per unit area from the profiles in Figure 12b. As result, Figure 13 shows the variation of the deduced exchange velocity V_{ex} (Eq. (7)) for different packing densities λ_p; the exchange velocities are normalized over the mean bulk flow velocity, U_b. It is observed that exchange velocities appear to be low (of the order of 0.005-0.01 of U_b) for the narrow canyon geometries with λ_p above 0.4; then exchange velocity appears to increase gradually to values of 0.03 of U_b as λ_p decreases to 0.3 (with the possible exception of the point at λ_p = 0.38). The observed difference in the exchange velocities across the investigated range of geometries does not seem to be linked to any change in the observed flow patterns within the cavity, as in all cases a recirculating cell occupies and extends across the canyon cavity (therefore confirming a skimming-flow regime). In the present study we find that the extent of the RSL thickness and specifically of the shear layer formed above the canopy layer affects the breathability. When the packing density is low (below 0.4), the shear layer above the canopy is very thin (less than 0.05H as seen from Figure 9) and as result the inertial sublayer essentially lies almost just above the canyon cavity enabling higher exchange of momentum flux and hence higher breathability of the urban area (Figures 9b and 13). When the packing density increases above 0.4, the shear layer grows thicker extending up to a further 0.6H (at λ_p = 0.7) above the canopy level, essentially almost isolating the cavity from the inertial sublayer, and diminishing the flux exchange at the canopy/canyon cavity level. As a result, the breathability reduces at the two most packed geometries by more than 80%. However, it is important to note that no matter how small, the existence of breathability makes a substantial qualitative difference for the urban atmosphere and their capacity for pollutant and heat removal. For the sake of comparison, it is noted that entrainment velocity/coefficient (which is the closest association to the exchange velocity referenced here) for free buoyant plumes is 0.08; therefore the range of variation of the exchange velocity in the urban atmosphere is not small comparatively.

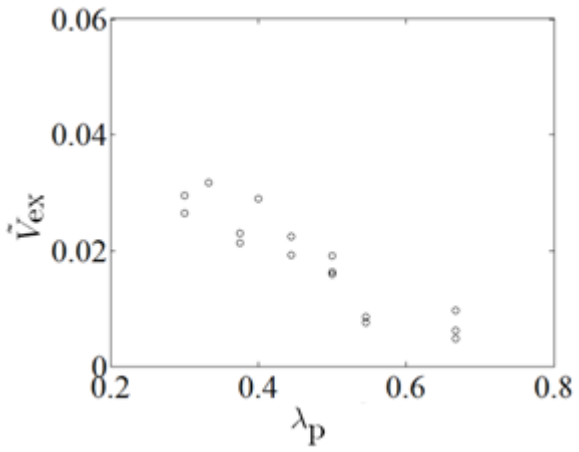

Figure 13: Variation of the non-dimensional exchange velocity (V_{ex}) (normalized with respect to U_b) with the

geometric packing density.

IV. CONCLUDING REMARKS

This paper investigates, in a series of laboratory experiments using PIV, the flow through and over two dimensional rectangular roughness elements arranged in a building-street canyon geometry. The resulting exchange processes between the flow within and above the canyon were investigated. The effect of the roughness elements packing density was also examined. The investigated values of packing densities, λ_p, ranged from λ_p = 0.30 to 0.67, reflecting typical European and North-American cities. The main conclusions from this work can be summarized as follows:

(a) Measurements of the velocity flow field (within and up to well above the street canyons) in the different geometries reveal that i) the mean flow within the canyon cavity (i.e., in-between roughness elements) consists of a dominant recirculation cell, whose basic form appears to persist throughout the investigated range of canyon geometries, and ii) that a shear layer develops and extends over the canyon cavity with its thickness varying depending on the packing density. The recirculation cell within the canyon appears to adjust to the geometrical packing density change, keeping a (close to) symmetric form in the range of geometries with λ_p ranging within $0.44 < \lambda_p < 0.55$ (or with $\lambda_p \approx 0.5 \pm 10\%$), but then shifting to a clearly asymmetric form (with its center displaced both vertically and horizontally) as the geometry deviates from the square cavity (i.e. from $\lambda_p = 0.5$, or $H/W = 1$).

(b) Measurements of the vertical Reynolds stress profiles gave insight into the variation of the roughness sublayer (RSL) thickness with the packing density of the roughness elements; the thickness of the RSL determines the thickness of the shear layer above the canopy layer, and in turn, the interaction (if any, depending on the packing density) between the inertial sublayer (ISL) and the flow within the roughness elements. Specifically, the thickness of the RSL was found to range from ~1.0H (min) at $\lambda_p = 0.3$ to 1.6H (max) $\lambda_p = 0.7$.When the packing density is low (below 0.4), the shear layer above the canopy is very thin (less than 0.05H) with the ISL essentially lying just above the canyon cavity and enabling thereby higher exchange of volume and momentum fluxes. When the packing density increases above 0.4, the shear layer grows thicker, extending up to a further distance of 0.6H (at $\lambda_p = 0.7$) above the canopy level, essentially almost isolating the cavity from the ISL.

(c) Based on the vertical profiles of the horizontal mean velocity and the Reynolds stress, the boundary layer scaling parameters were deduced – the surface roughness length, z_0, the zero-plane displacement thickness d_0 and the friction velocity, u_* - as a function of the packing density of the roughness elements. It is noted that the lowest friction velocities (~0.1, normalized over the bulk velocity) are exhibited both for the highest- and lowest-packed geometries (i.e. for λ_p <0.4 and for $\lambda_p > 0.55$) while in the medium-packed geometries ($0.44 < \lambda_p < 0.55$) the friction velocities are relatively highest (~0.15-0.2). This variation reflects the turbulence variation with the packing density change.

(d) The exchanged fluxes at the urban canopy top level was characterized and quantified by a mean exchange velocity in a similar fashion to the concept of an entrainment velocity. The reported exchange velocity values were normalized over the mean bulk velocity. These were found to range (monotonically) from 0.03 for the sparser geometries (e.g., $\lambda_p = 0.33$) to ~0.0075 for the denser geometries (e.g., $\lambda_p = 0.67$). This result corresponds to a reduction in the *breathability* capacity of the denser roughness packing (or city) by more than 50%. This variation reflects more the mean velocity shear variation with the packing density.

ACKNOWLEDGEMENTS

MKAN wishes to acknowledge funding from the Cyprus Research Promotion Foundation with contract number ΑΝΑΒΑΘΜΙΣΗ/ΠΑΓΙΟ/0308/33. MKAN and CNM would also like to acknowledge Dr. I. Zadrazil and Dr. C. Marakkos for their support in PIV data post-processing and figure/image production. MKAN also acknowledges stimulating discussions with Prof. R. E. Britter of the Massachusetts Institute of Technology (US) and Prof. H. J.S. Fernando of the University of Notre Dame (US).

REFERENCES

[1]H. Schlichting and K. Gersten, Boundary Layer Theory, 8th Edition (Springer-Verlag, Berlin, 2000).

[2]T.B. Nickels. IUTAM Symposium on The Physics of Wall-Bounded Turbulent Flows on Rough Walls, held Cambridge, UK, 7-9 July 2009; Springer, IUTAM Bookseries **22** (2010); ISBN 978-90-481-9630-2.

[3]O. Cadot, D. Bonn, and S. Douady, "Turbulent drag reduction in a closed flow system: Boundary layer versus bulk effects," Phys. Fluids **10**, 426 (1998).

[4]A. Ferrante and S. Elghobashi, "On the physical mechanisms of drag reduction in a spatially developing turbulent boundary layer laden with microbubbles," J. Fluid Mech. **503**, 345 (2004).

[5]J. R. Garratt, The Atmospheric Boundary Layer, Cambridge Atmospheric and Space Science Series (Cambridge University Press, Cambridge, 1992).

[6]C. Gordon, "Intermittent momentum transport in a geophysical boundary layer," Nature **248**, 392 (1974).

[7]R. E. Britter, and S. R. Hanna, "Flow and dispersion in urban areas," Ann. Rev. Fluid Mech. **35**, 469 (2003).

[8]M.K.-A. Neophytou, D. Goussis, E. Mastorakos, and R. E. Britter, "The development of a scale-adaptive reactive pollutant dispersion model," Atmos. Environ. **39**, 2787 (2005).

[9]H. J. S. Fernando, "Fluid mechanics of urban atmospheres in complex terrain," Annu. Rev. Fluid Mech. **42**, 365 (2010).

[10]H. J. S. Fernando, D. Zajic, S. DiSabatino, R. Dimitrova, B. Hedquist, and A. Dallman, "Flow, turbulence and pollutant dispersion in urban atmospheres," Phys. Fluids **22**, 051301 (2010).

[11]C. S. B. Grimmond and T. R. Oke, "Aerodynamic properties of urban areas derived from analysis of surface form," J. Appl. Meteorol. **38**, 1262 (1999).

[12]J. R. Garratt, "Surface influence upon vertical profiles in the atmospheric near-surface layer," Quart. J. Roy. Meteorol. Soc. **106**, 803 (1980).

[13]R. W. Macdonald, R. F. Griffiths, and D. J. Hall, "An improved method for the estimation of surface roughness of obstacle arrays," Atmos. Environ. **32**, 1857 (1998).

[14]H. Cheng and I. P. Castro, "Near wall flow over urban-like roughness," Bound.-Layer Meteorol. **104**, 229 (2002).

[15]H. Cheng, P. Hayden, A.G. Robins, and I. P. Castro, "Flow over cube arrays of different packing densities," J. Wind Eng. Ind. Aerodyn. **95**, 715 (2007).

[16]R. A. Antonia and P.-Å Krogstad. "Turbulence structure in boundary layer over different type of surface roughness," Fluid Dyn. Res. **28**, 139 (2001).

[17]P.-Å. Krogstad and V. Efros, "About turbulence statistics in the outer part of a boundary layer developing over two-dimensional surface roughness," Phys. Fluids **24**, 075112 (2012).

[18]M. J. Brown, R. E. Lawson, D. S. Descroix, and R. L. Lee, "Mean flow and turbulence measurements around a 2-D array of buildings in a wind tunnel," in Proceedings of the 11th Joint Conference on Applications of Air Pollution Meteorology with the Air and Waste Management Association, American Meteorological Society, 9-14 January 2000, Long Beach, CA, USA (2000), ID #63740, U.S, Environmental Protextion Agency, Office of Research and Development, National Exposure Research Lab, Atmospheric Modelling Division, Applied Modelling Research Branch.

[19]P.-Å. Krogstad, R. A. Antonia, and L. W. B. Browne, "Comparison between rough- and smooth-wall turbulent boundary layers," J. Fluid Mech. **245**, 599 (1992).

[20]K. A. Flack, M. P. Schultz, and J. S. Connelly, "Examination of a critical roughness height for outer layer similarity," Phys. Fluids **19**, 095104 (2007).
[21]S. Leonardi. P. Orlandi. R. J. Smalley, L. Djenidi, and R. A. Antonia, "Direct numerical simulations of turbulent channel flow with transverse square bars on one wall," J. Fluid Mech. **491**, 229 (2003).
[22]P. Kastner-Klein, R. Berkowicz, and R. Britter, "The influence of street architecture on flow and dispersion in street canyons," Meteorol. Atmos. Phys. **87**, 121 (2004).
[23]P. Kastner-Klein and M. W. Rotach, "Mean flow and turbulence characteristics in an urban roughness sublayer," Bound.-Layer Meteorol. **111**, 55 (2004).
[24]I. Eliasson, B. Offerle, C. S. B. Grimmond, and S. Lindqvist, "Wind fields and turbulence statistics in an urban street canyon," Atmos. Environ. **40**, 1 (2006).
[25]M. W. Rotach, "Turbulence close to a rough urban surface part II: Variances and gradients," Bound.-Layer Meteorol. **66**, 75 (1993).
[26]M. W. Rotach, "Profiles of turbulence statistics in and above an urban street canyon," Atmos. Environ. **29**, 1473 (1995).
[27]P. Louka, S. E. Belcher, and R. G. Harrison, "Coupling between air flow in streets and the well-developed boundary layer aloft," Atmos. Environ. **34**, 2613 (2000).
[28]S. E. Belcher, "Mixing and transport in urban areas," Phil. Trans. R. Soc. A **363**, 2947 (2005).
[29]T. Bentham and R. Britter, "Spatially averaged flow within obstacle arrays," Atmos. Environ. **37**, 2037 (2003).
[30]D. Hamlyn and R. Britter, "A numerical study of the flow field and exchange processes within a canopy of urban-type roughness," Atmos. Environ. **39**, 3243 (2005).
[31]I. Panagiotou, M. Neophytou, D. Hamlyn, and R. Britter "City breathability as quantified by the exchange velocity and its spatial variation in real inhomogeneous urban geometries: An example from central London urban area," Sci. Total Environ. **442**, 466 (2013).
[32]M. Neophytou, A. Gowardan, and M. J. Brown, "An inter-comparison of three urban wind models using Oklahoma City Joint Urban 2003 wind field measurements," J. Wind Eng. Ind. Aerodyn. **99**, 357 (2011)
[33] F. Caton, R. E. Britter, and S. Dalziel, "Dispersion mechanisms in a street canyon," Atmos. Environ. **37**, 693 (2003).
[34]J. F. Barlow, I. N. Harman, and S. E. Belcher, "Scalar fluxes from urban street canyons. Part I: Laboratory simulation," Bound.-Layer Meteorol. **113**, 369 (2004).
[35]L. Soulhac, R. J. Perkins, and P. Salizzoni, "Flow in a street canyon for any external wind direction," Bound.-Layer Meteorol. **126**, 365 (2008).
[36]P. Salizzoni, L. Soulhac, and P. Mejean, "Street canyon ventilation and atmospheric turbulence," Atmos. Environ. **43**, 5056 (2009).
[37]X.-X. Li, D. Y. C. Leung, C.-H. Liu, and K. M. Lam, "Physical modeling of flow field inside urban street canyons," J. Appl. Meteorol. Climatol. **47**, 2058 (2007).
[38]M. Princevac, J. J. Baik, X. Li, H. Pan and S.-B. Park, "Lateral channelling within rectangular arrays of cubical obstacles," J. Wind Eng. Ind. Aerodyn. **98**, 377 (2010).
[39]I. Harman, J. Barlow, and S. Belcher, "Scalar fluxes from urban street canyons. Part II: Model." Bound.-Layer Meteorol. **113**, 287 (2004).
[40]Y. Yang, and Y. Shao, "A scheme for scalar exchange in the urban boundary layer," Bound.-Layer Meteorol.

120, 111 (2006).

[41]C.-H. Liu, D. Y. C. Leung, and M. C. Barth, "On the prediction of air and pollutant and exchange rates in canyons of different aspect ratios using large-eddy simulation," Atmos. Environ. **39**, 1567 (2005).

[42]P. Orlandi, S. Leonardi, R. Tuzi, and R. A. Antonia, "Direct numerical simulation of turbulent channel flow with wall velocity disturbances," Phys. Fluids **15**, 3587 (2003).

[43]M. Motozawa, T. Ito, K. Iwamoto, H. Kawashima, H. Ando, T. Senda, Y. Tsuji, Y. Kawaguchi, "Experimental investigations on frictional resistance and velocity distribution of rough wall with regularly distributed triangular ribs," Int. J. Heat Fluid Flow, **41**, 112 (2013).

[44]T. Ito, A. Matsumoto, T. Ito, M. Motozawa, K. Iwamoto, H. Kawashima, T. Senda, and Y. Kawaguchi, "Experimental investigation on effects of surface roughness geometry affecting to flow resistance," Proc. ASME-JSME-KSME Joint Fluid Engineering Conference: Volume 1, Symposia – Parts A,B,C,D, Hamamatsu, Japan, July 24-29 (2011). ISBN: 978-0-7918-4440-3

[45]R. N. Meroney, M. Pavageau, S. Rafailidis, and M. Schatzmann, "Study of line source characteristics for 2-D physical modelling of pollutant dispersion in street canyons," J. Wind Eng. Ind. Aerodyn. **62**, 37 (1996).

[46]W. G. Hoydysh, R. A. Griffiths, and Y. Ogawa, "A scale model study of the dispersion of pollution in street canyons," APCA Paper No. 74-157. In: 67th Annual Meeting of the Air Pollution Control Association, Denver, CO, June 9-13 (1974).

[47]W. H. Snyder, "Similarity criteria for the application of fluid models to the study of air pollution meteorology," Bound.-Layer Meteorol. **3**, 113 (1972).

[48]T. R. Oke, Boundary Layer Climates, (Routledge, London, 1988).

[49]T. R. Oke, "Street design and urban canopy layer climate," Energy Build. **11**, 103 (1988).

[50]M. R. Raupach, "A wind-tunnel study of turbulent flow close to regularly arrayed roughness element," Boundary-Layer Meteorol. **18**, 373 (1980).

[51]R. W. Macdonald, "Modelling the mean velocity profile in the urban canopy layer," Boundary-Layer Meteorol. **97**, 25 (2000).

[52]S. Oikawa and Y. Meng, "Turbulence characteristics and organized motion in a suburban roughness sublayer," Bound.-Layer Meteorol. **74**, 289 (1995).